Intrinsic Point Defect Clustering During Czochralski Growth of (Silicon and) Germanium

Jan Vanhellemont[1] and Piotr Śpiewak[2]

[1]Department of Solid State Sciences, Ghent University
Krijgslaan 281-S1, B-9000 Gent, Belgium
jan.vanhellemont@ugent.be

[2]Materials Design Division
Faculty of Materials Science and Engineering
Warsaw University of Technology
Wooska 141, 02-507 Warsaw, Poland
pspiewak@inmat.pw.edu.pl

Abstract

An overview is given on recent progress in understanding intrinsic point defect clustering during Czochralski growth of silicon and germanium. The similarities and differences between both semiconductors are discussed with special emphasis on germanium. Recent theoretical and experimental results on the thermodynamical properties of the vacancy in germanium are presented. Quenching experiments in combination with analytical and ab initio calculations are used to estimate the vacancy formation energy and the thermal equilibrium concentration of vacancies in germanium. The impact of doping silicon with Ge during Czochralski crystal growth on vacancy equilibrium concentration and grown-in void density is discussed.

1   Introduction

Due to its high carrier mobility, there is a renewed interest to use germanium as active semi-conducting layer in advanced electronic devices on silicon substrates [1]. In addition doping of silicon crystals with a sub percentage concentration of germanium can be used to improve both silicon crystal and wafer properties, see e.g. Vanhellemont et al [2] and references therein.

Successful Czochralski (Cz) single crystal growth and device processing of germanium requires a much better understanding of its intrinsic point defect properties than is available at present. As it will be shown a lot can be learned from the experience and comparison with silicon.

Experimental data on e.g. the thermal equilibrium concentration of vacancies in germanium are scarce and most are more than 40 years old. Most of the experimental data were obtained using quenching experiments. It is assumed that the number of quenched-in acceptors that are formed during the fast cooling are directly proportional to the number of vacancies before the quenching. Under this assumption, the vacancy concentration at the anneal temperature can be estimated from the measured resistivity changes. A compilation of available published

results can be found elsewhere [3]. Recently, a novel quenching technique to study vacancy properties in silicon has been developed [4] that has also be applied with success to Ge doped silicon wafers [5].

The formation energy of the vacancy in its different charge states in silicon and germanium have been calculated using the CASTEP [6] and VASP (with LDA+U approximation and also with hybrid functionals) [7, 8] codes. For germanium, these results show a remarkably good agreement between the calculated formation energy of the (double) negatively charged vacancy and the measured formation energy of quenched-in defects. Also the deep levels in the bandgap associated with the different charge states of the vacancy are very well reproduced.

2 Previous experimental studies of the thermodynamic properties of the vacancy in silicon and germanium

During the 1950' and 60's, quenching experiments have been used extensively to study intrinsic point defect properties in germanium [9, 10, 11, 12, 13, 14, 15, 16]. Quenching of germanium from high temperatures leads to the formation of acceptors which change the resistivity of the sample. Using Hall effect and four point probe resistivity measurements, the concentration of the acceptors can de determined as function of the quenching temperature and from this the formation energy and the thermal solubility can be obtained. A wide range of acceptor concentrations was observed in the different quenching experiments. The extracted acceptor formation energy E^F, however, was in all cases quite similar and close to $2eV$. As was the case for quenching experiments on metals, it was assumed that the acceptors were related to quenched-in vacancies. A compilation of these old results and a first comparison with results of analytical and ab initio calculations was given in [3]. In the 80's, Kamiura et al [17, 18, 19] performed detailed studies of the defects in quenched germanium using beside Hall effect measurements also analytical techniques that were not available previously. DLTS and Photo Thermal Ionization Spectroscopy (PTIS) were used to study the levels in the bandgap associated with the quenched in defects. They showed that in many of their experiments, Cu contamination played an important role in the acceptors formed by quenching.

A constant concern in all of these quenching experiments has indeed been the risk of introducing unintentionally Cu contamination during the high temperature anneal. Substitutional Cu has also a solubility energy of around $2eV$, behaves as a triple acceptor and therefor will lead to similar changes of the resistivity after the quenching step. Substitutional Cu is a triple acceptor with levels at $E_V + 0.04eV$, $E_V + 0.32eV$ and $E_C - 0.26eV$, identified by Hall effect [20] and later confirmed with DLTS [21, 22].

In the early days already quenching from high temperatures has been explored to study the intrinsic point defects in Si. It was indeed observed that by quenching from high temperatures, donors are formed which change the resistivity of the Si material and can easily be detected using resistivity and Hall measurements. Unfortunately, it soon turned out that in most cases these donors were due to iron contamination either grown-in during crystal growth and activated by the quenching treatment or diffusing in from the surface of the samples during the high temperature treatment [23]. Often the concentration of iron was so high that it was the main cause of the observed resistivity changes. Only in few careful studies also donors were observed that could not be related to metallic impurities [24, 25] but even in these cases the relation with the intrinsic point defects was not clear.
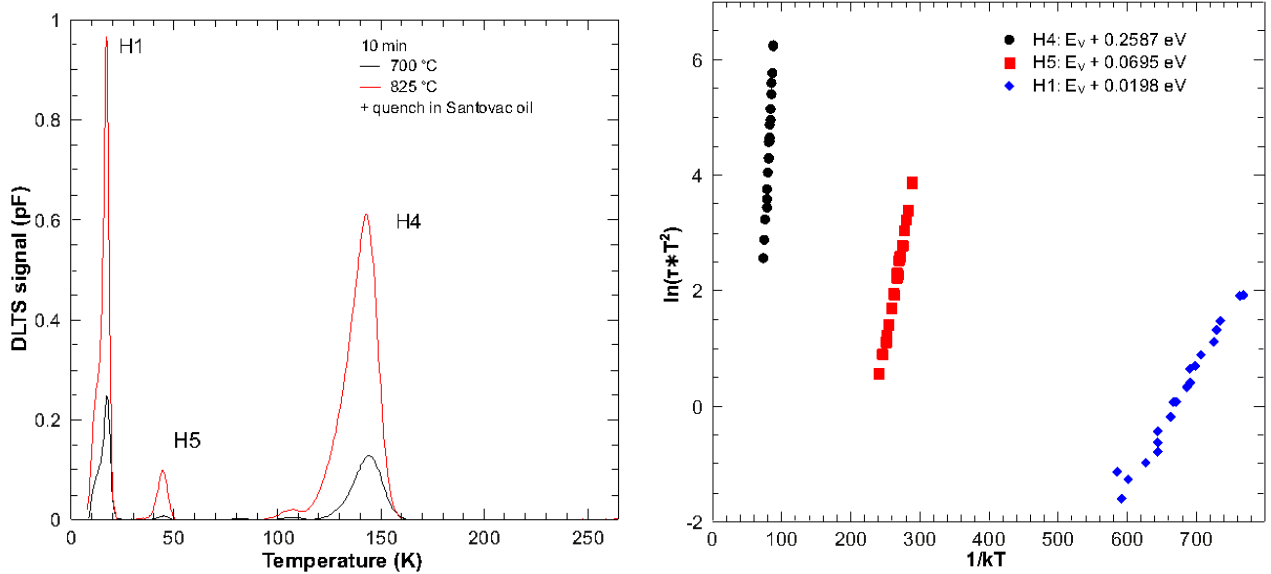
Figure 1: **Left**: Typical DLTS spectra measured in samples quenched in Santovac 5 oil after a 10 min anneal at 825 °C and in silicon oil after a 10 min anneal at 700 °C. No known Cu-related deep levels are observed. **Right**: Arrhenius plot of the deep levels $H1$, $H4$ and $H5$ [27].

3 Recent quenching experiments

3.1 Quenching experiments on germanium

In the present study 750 μm thick, p-type, 18 Ωcm germanium samples were annealed for various times and then quenched in different quenching liquids. To avoid metal contamination, the samples were carefully cleaned before the high temperature treatment. After rinsing in high purity methanol, they were etched for 1 min in $HF - HNO_3$ (1:3), followed by rinsing in distilled water and finally again in methanol. Some of the samples were treated in a Rapid Thermal Annealing (RTA) furnace which revealed that also in that case thermal acceptors were formed during the rapid cooling.

After quenching, the acceptor concentration was determined using Hall effect and four point probe resistivity measurements yielding a formation energy of about $1.97 \pm 0.21 eV$ and a prefactor of $9 \times 10^{24} cm^{-3}$ [26, 27].

Some of the samples were also analyzed with Deep Level Transient Spectroscopy (DLTS) to determine the deep levels associated with the acceptors and to verify that metal contamination is sufficiently low. Typical DLTS results for samples quenched in Santovac 5 oil (polyphenol ether) are shown in Fig. 1 together with the Arrhenius plots for the three observed levels. The dominant deep levels $H1$ and $H4$ which occur with a concentration comparable to the acceptor concentration derived from the electrical measurements, do not correspond with known metal related deep levels. In RTA treated samples, also Cu related deep levels were however observed besides the $H1$ and $H4$ levels with comparable concentrations. FTIR analyses were performed in order to obtain more information on the nature of the quenched-in defects and show besides the known quenched in defects also the presence of substitutional Cu.

In the samples quenched in Santovac 5 oil, FTIR analyses revealed not only the presence of the first acceptor level of substitutional Cu but also up to three shallower quenched-in acceptors, i.e. the SA2 and SA3 acceptors already observed with PTIS by Broeckx et al [28]
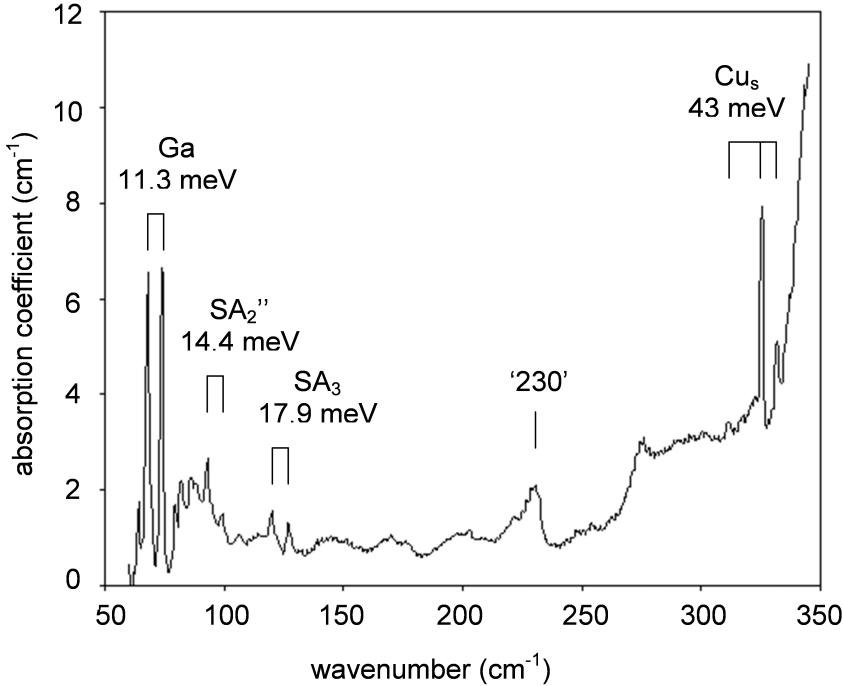
Figure 2: FTIR spectrum of a sample quenched from $825°C$ in Santovac 5 oil. Beside the acceptor series from substitutional Cu and from the Ga dopant, also absorption lines are seen from semi-shallow quenched-in acceptors [27].

and an absorption band around 230 cm^{-1} that was observed by Hattori et al [29] in Cu-doped and quenched or irradiated germanium. These semi-shallow acceptors correspond with band $H1$ observed with DLTS, confirming that $H1$ is different from the band due to the 0.04 eV level of substitutional Cu which has a higher temperature position. A typical FTIR spectrum is shown in Fig. 2. The fact that Cu is not observed in the DLTS spectra obtained on the same samples might be related to the fact that DLTS only probes a near surface layer of up to about 10 μm thickness which might be depleted of Cu due to outdiffusion.

3.2   Quenching experiments on germanium doped silicon

After a 1h anneal in hydrogen atmosphere at the quench temperature that is varied between 1200 and 1350°C, germanium doped silicon samples were quenched in water at room temperature and a 1 h anneal was performed at 450°C in order to transform most of the V_mH_n complexes in VH_4. The VH_4 concentration was determined by FTIR measuring the intensity of the 2223 cm^{-1} peak that is due VH_4. Hereby it is assumed that the concentration of VH_4 is proportional to the vacancy concentration at the temperature before quenching [5].

The quenching temperature dependence of the intensity of the 2223 cm^{-1} peak for high resistivity FZ-grown (HRFZ) and magnetic field assisted Cz -grown (MCZ) silicon [4] and for Ge doped Cz silicon is shown in Fig. 3, revealing for HRFZ an Arrhenius type dependence of the peak intensity I_{VH_4} on temperature T, that can be described by [5]

$$I_{VH_4} = I_{VH_4}^0 e^{-\frac{E_V^F}{kT}}, \tag{1}$$

with E_V^F the apparent vacancy formation energy and k the Boltzmann constant. The pre-factor $I_{VH_4}^0$ includes both the formation entropy and the infra red calibration coefficient.

When a vacancy trapping species exists with a formation energy E_T, (1) can in first order approximation be rewritten as

$$I_{VH_4} \approx (1 - Ae^{-\frac{E_T}{kT}})I_{VH_4}^0 e^{-\frac{E_V^F}{kT}}. \tag{2}$$
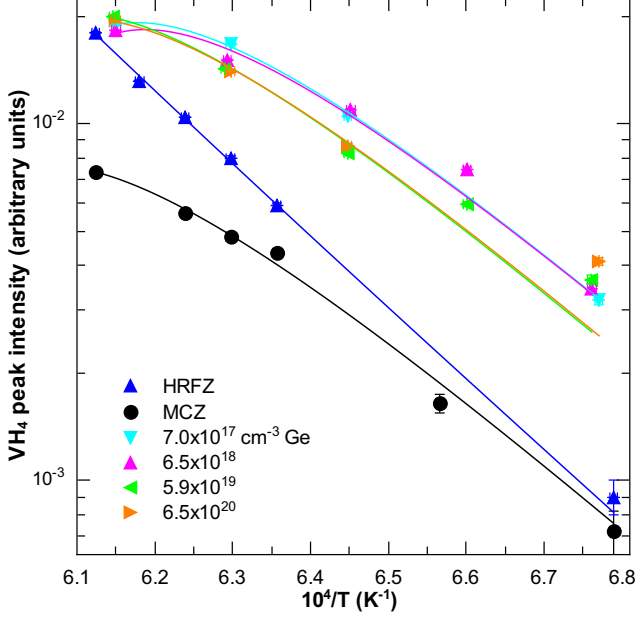
4

Figure 3: Quenching temperature dependence of the peak intensity of the 2223 cm^{-1} absorption band after the 450°C anneal for the four Ge concentrations studied [5]. Results for HRFZ and MCZ silicon [4] are also shown as a reference. The lines are best fits using (2).

Using (2) to fit the MCZ data shown in Fig. 3 assuming that $E_V^F = 3.85$ eV and $E_T = E_{VO} = 1.85$ eV, reproduces well the observed dependence of the vacancy concentration on the quenching temperature. When applying (2) to the HRFZ data, an excellent fit is also obtained and one should note that the resulting value A is about one order of magnitude smaller than that for the MCZ and Ge doped Cz materials, in agreement with the oxygen content which is also one order of magnitude lower. It is also interesting to note that the pre-factor $I_{VH_4}^0$ for HFRZ and MCZ is nearly the same, suggesting that the observed apparent vacancy formation energy in MCZ is fully due to the trapping of vacancies by oxygen.

4 Analytical estimation of the vacancy formation energy in germanium

The theory developed by Kröger [30] can be used to estimate the formation energy of the vacancy in different charge states when the deep levels associated with the charged point defect are known [3]. The ratio between the concentrations of neutral and of single negatively charged vacancies is indeed given by

$$\frac{C_{V^0}^*}{C_{V^{1-}}^*} = \frac{1}{2} \left(\frac{f_T g_c}{g_v} \right)^{\frac{1}{2}} \left(\frac{m_e^*}{m_h^*} \right)^{\frac{3}{4}} e^{\frac{\frac{1}{2} E_g^0 - E_A}{kT}}, \tag{3}$$

while the ratio between the concentrations of double and single negatively charged vacancies is given by

$$\frac{C_{V^{2-}}^*}{C_{V^{1-}}^*} = \frac{1}{2} \left(\frac{g_v}{f_T g_c} \right)^{\frac{1}{2}} \left(\frac{m_e^*}{m_h^*} \right)^{\frac{3}{4}} e^{\frac{E_{A2-} - \frac{1}{2} E_g^0}{kT}}. \tag{4}$$

$f_T = 164$ is a factor resulting from the temperature dependence of the bandgap E_g, $g_v = 1$ and $g_c = 4$ are the multiplicity of the valence and conduction band, m_e^* and m_h^* are the effective masses of electrons and holes with $\frac{m_e^*}{m} = 0.11$ and $\frac{m_h^*}{m} = 0.33$, $E_g^a = 0.785 eV$ is the width of the band gap at 0K. Assuming that deep levels $H1$ and $H4$, observed by DLTS, are due to the single and double negative charge states of the vacancy, one has $E_A = 0.02 eV$ and

$E_{A^{2-}} = 0.26eV$. Equations (3) and (4) suggest that the formation energy of the uncharged vacancy would be $0.37eV$ higher than that of the single negatively charged vacancy, while that of the double negatively charged vacancy would be $0.13eV$ lower, in contrast to the results presented in [3] where $E_{A^{2-}} = 0.6eV$ was used, as was also done by Kröger [30]. The thermal equilibrium vacancy concentration $C^*_{V^x}$ (with $x = 0, 1-$ and $2-$, for the uncharged, single and double negatively charged vacancy, respectively) is given by

$$C^*_{V^x} = C^0_{V^x} e^{-\frac{E^F_{V^x}}{kT}}. \tag{5}$$

The highest concentration of thermal vacancies was obtained in the experiments of Samuelsson [15] who also used the most aggressive quenching technique by quenching the samples in methanol at dry ice temperature thus minimizing vacancy out-diffusion and clustering during cooling. Assuming that the obtained resistivity changes were mainly due to quenched-in double negatively charged vacancies, one can also estimate the solubility of the single negatively charged and the neutral vacancy using equations (3) and (4). Based on diffusion experiments Brotzmann and Bracht [31] recently concluded also that the double negatively charged vacancy is the dominant intrinsic point defect in germanium. It should be noted however that the equilibrium concentrations, for charged vacancies, hold for near intrinsic conditions. As illustrated by the ab initio calculations discussed in the next paragraph, high dopant concentrations change the formation energies of charged vacancies and thus also the corresponding solubilities .

5 Ab initio calculations of vacancy properties

Density Functional Theory (DFT) calculations have been extensively used the last years to calculate the thermodynamic properties of the intrinsic point defects in germanium. One important shortcoming of DFT calculations based on the local density approximation (LDA) or the generalized gradient approximation (GGA), is the failure to reproduce well the band-gap of semiconductors and insulators. In the case of germanium, a closing of the band gap is even observed for well-converged DFT calculations [32] predicting thus a metallic ground state which obviously does not correspond with reality. Using the LDA and introducing an on-site Coulomb interaction U correction (LDA+U), leads to a partial opening of the band gap [7]. This correction is performed by adding an orbital-dependent term in a (screened) Hartree-Fock like manner to the LDA potential. LDA+U thus allows to calculate the formation energies of the different charge states of the self-interstitial and the vacancy in germanium yielding formation energies of 2.0, 2.05 and 2.33 eV for V^{2-}, V^{1-} and V^0, respectively, when assuming the Fermi level at half bandgap [7]. Recently it was proposed to use the hybrid functional HSE06 which should give a more accurate estimate of the formation energy as the occupation of the defect bands is better described. The dependence of the formation energies on the position of the Fermi level for both calculation approaches is shown in Fig. 4. The results are in good agreement with those of the analytical calculation in the previous paragraph. At the same time, due to the opening of the bandgap by the both approximations, the associated deep levels can be calculated and two acceptor levels were obtained, i.e. 0.02 and 0.26 eV, for the $V^{0/1-}$ and $V^{1-/2-}$ transitions, respectively. This is also in amazing agreement with the DLTS observations (levels H1 and H4, respectively).
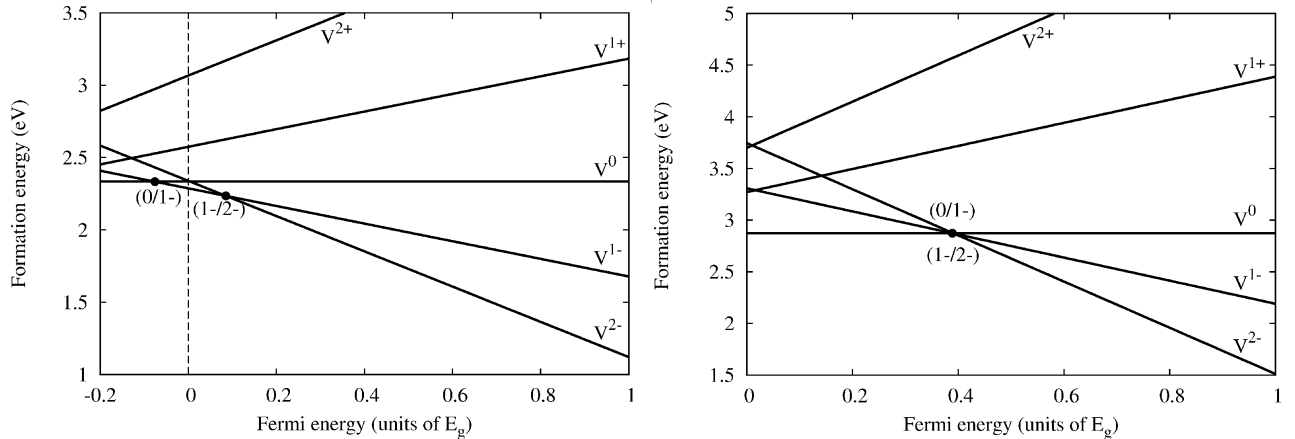
Figure 4: The calculated formation energy of the vacancy in germanium as a function of its charge state and the position of the Fermi level. The formation energies are calculated using the $LDA + U$ method (**left**) and the hybrid functional HSE06 (**right**) [7, 8].

6 Diffusivity of vacancies and self-interstitials

In silicon, self-interstitials diffuse faster at high temperatures than vacancies while the equilibrium concentration of vacancies is higher than that of self-interstitials. Figure 7 shows the temperature dependence of Si self-diffusivity determined by SIMS [33] and Raman scattering [34] of isotope heterostructures.

As illustrated in the figure, the measured self-diffusion coefficient D_{Si}^{SD} can be fitted well by

$$D_{Si}^{SD} = 2175.4 exp(-\frac{4.95eV}{kT}) + 0.0023 exp(-\frac{3.6eV}{kT}) cm^2 s^{-1}. \tag{6}$$

The first term in (6) is the self-interstitial contribution while the second term describes the vacancy related part.

The right part of Figure 7 shows the literature data on Ge self-diffusivity [35, 36, 38, 37]. These data points can accurately be described by a single activation enthalpy and a pre-exponential factor by [35]

$$D_{Ge}^{SD} = 25.4 exp(-\frac{3.13eV}{kT}) cm^2 s^{-1}. \tag{7}$$

The Arrhenius behavior implies that vacancy diffusion controls self-diffusion in germanium crystals over the entire temperature range of interest and that there is no noticeable self-interstitial contribution [35]. Therefore, for germanium

$$C_I^{eq} D_I << C_V^{eq} D_V. \tag{8}$$

7 MD calculation of vacancy cluster formation

The properties of small vacancy clusters are difficult to determine experimentally. On the other hand, it is also difficult to study these properties using ab initio and tight-binding atomistic calculations, due to large computational efforts required for these techniques, in the case of a large atomistic domains. These limitations can be circumvented by classical molecular dynamics
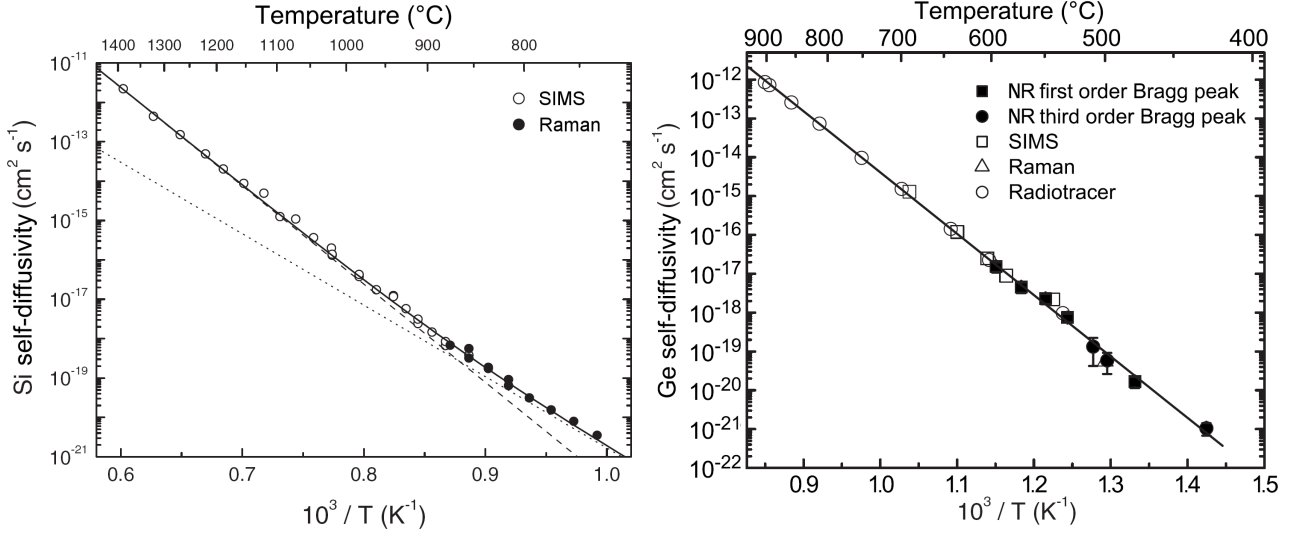
Figure 5: Temperature dependence of the Si (left) and Ge (right) self-diffusivity in intrinsic material [8]. **Left**: The temperature dependence of the Si self-diffusivity was measured by SIMS [33] (open circles) and Raman scattering [34] (solid circles) of isotope heterostructures. The solid line is the best fit using (6). The contributions of the self-interstitial and vacancy mechanism are shown by the dashed and doted lines, respectively [34]. **Right**: The temperature dependence of the Ge self-diffusivity was measured by neutron reectometry (NR) [35] (solid circles and squares), SIMS [36] (open squares) and Raman scattering [37] (open triangle) of isotope heterostructures and radiotracer [38] diffusion measurements. The solid line is the best fit using (7).

(MD) calculations, based on a Stillinger and Weber potential, which were used for a theoretical investigation of growth patterns of vacancy agglomerates V_i, in the range $1 \leq i \leq 35$ [8].

In order to avoid cluster dissociation, all MD calculations were performed for a constant temperature of 300 K, under the NVT-ensemble with periodic boundary conditions. First,the equilibrium enthalpy of the system was calculated for a perfect lattice consisting of 1728 atoms. These calculations are then repeated for the same structure with a number of vacancies. A sequence of ten runs, each containing of 70000 steps (corresponding to 11 ps of real time) were performed for each cluster size and configuration. The results were subsequently averaged to minimize statistical uncertainty.

It should be noted that, the short time scale of MD calculations is sufficient only for localized lattice relaxation, not for long-ranged diffusive rearrangement of cluster geometry. As a result, the choice of the initial cluster geometry is critically important for making conclusions regarding nucleation and growth pathways [39, 40].

Three cluster growth modes, shown in Figure 6, were investigated in order to find the energetically favorable mode. The choice of these growth modes was based on the results of the previous work, on vacancy cluster growth in silicon single crystals [39, 40, 41, 42, 43]. In the first case, Ge atoms are removed from the six-member ring and ten-member cage structures in the diamond lattice. In this way octahedral-like vacancy clusters are formed called here hexagonal ring clusters (HRC). In the second case, the successive shells on neighbors of a given Ge atom were taken out in order to form spherically shaped clusters (SPC). The third investigated cluster growth mode was the (111)-oriented stacking fault (SF), which consists of interconnected six-member vacancy ring arranged in a (111) plane.
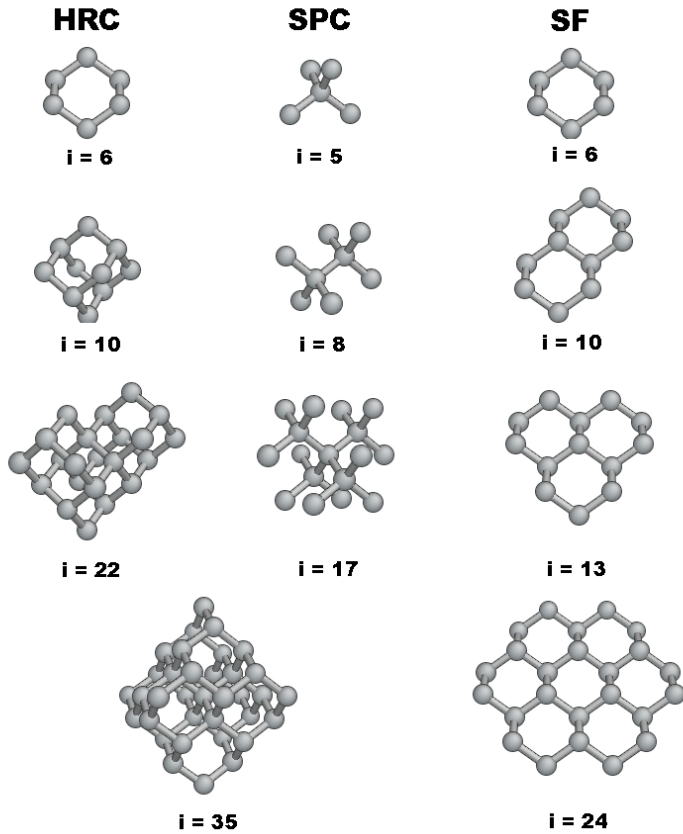
Figure 6: Configuration of vacancy cluster growth modes in germanium for the HRC-6, 10, 22 and 35, the SPC-5, 8, 17 and 35, and the SF-6, 10, 13 and 24 vacancy clusters [8].

The energetically favorable growth mode was determined by comparing the formation energies for clusters containing between 1 and 35 vacancies. The formation energy for a cluster which contains i vacancies can be calculated from

$$E^f(i) = E(N - i) - \frac{N - i}{N} E(N). \tag{9}$$

$E(N)$ is the energy of a perfect system with N atoms and $E(N - i)$ is the energy of a system with $N - i$ atoms (lattice with N sites and i vacancies). The results of these calculations shown in Figure 7, demonstrate that SF clusters have a higher formation energy than the HRC and SPC ones, so that their formation is less likely. The formation energies for spherically shaped and hexagonal ring clusters seem to intersect one the other, similar as in the case of silicon [41]. Such behavior suggests that the agglomeration mechanism for large vacancy clusters is rather complex and SPC and HRC clusters are competing.

7.1 Dependence of surface energy on cluster size

Continuum models describing void formation and growth use a phenomenological expression for the vacancy cluster formation energy of the form

$$E^f(i) = \sigma i^{\frac{2}{3}}, \tag{10}$$

where σ is an effective surface energy for a cluster containing i vacancies. Fitting the formation enthalpies for vacancy clusters in germanium lattice (for HRC and SPC vacancy agglomerates) with the same power-law results in following equation [8]
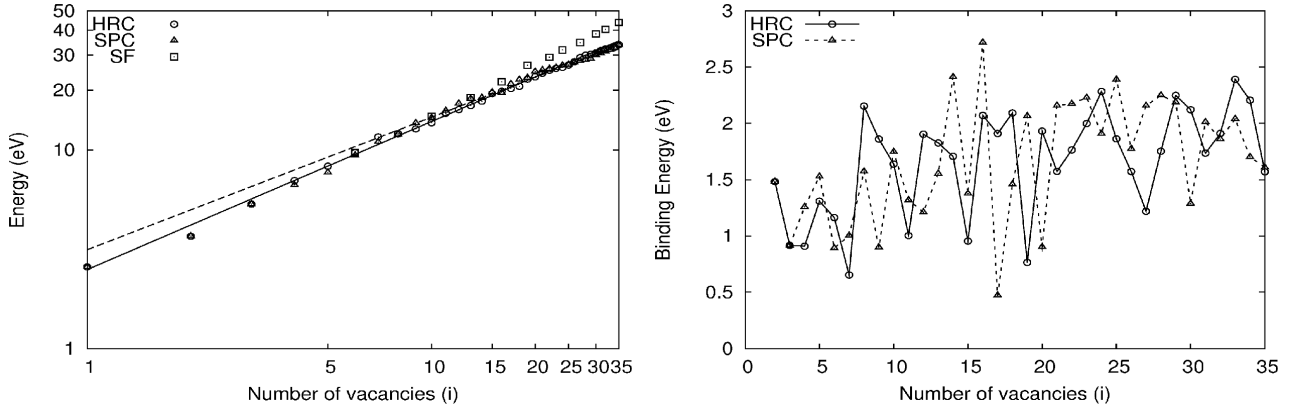
Figure 7: **Left**: Formation enthalpies of HRC, SPC and SF vacancy clusters in single crystal germanium as a function of the number of vacancies i in the cluster - the dashed line shows the power-law fit $(\sigma i^{\frac{2}{3}})$ and the solid line the correction (optimal fit) for the cluster size interval $1 \leq i \leq 19$ for the HRC and SPC clusters. **Right**: Binding energy of HRC and SPC vacancy clusters in germanium as a function of the cluster size i [8].

$$E^f(i) = 3.15i^{\frac{2}{3}}eV. \tag{11}$$

This phenomenological expression for cluster energy is most accurate for a cluster size $i > 20$, because smaller clusters deviate from the classical $i^{\frac{2}{3}}$ energy scaling behavior. The pre-factor 3.15 corresponds with a surface energy of 1.1 J/m_2 (at 0 K)when assuming octahedral voids. This is value is close the 1.05 J/m_2 value that was obtained for silicon [39].

For smaller vacancy clusters containing less then 20 vacancies, the MD calculations suggest that another expression for the vacancy cluster formation energy should be used. For the size interval $1 \leq i \leq 19$, the best fit is obtained for [8]

$$E^f(i) = 2.50i^{0.745}eV. \tag{12}$$

Equation (12) can be used to increase the accuracy of continuum models, which use phenomenological expression for the vacancy cluster formation energy. The exponent of 0.745 is in between 1 that is valid for stacking faults and 2/3 that is valid for spheres, (truncated) octahedra or other clusters with constant aspect ratio. It could be explained by assuming that the aspect ratio of the cluster is changing from the one of a nearly plate-like shape for the smallest clusters to the one of more spherical or octahedral shapes for larger clusters.

7.2 Dependence of vacancy binding energy on cluster size

The relative stability of vacancy clusters was investigated in terms of their binding energy. The binding energy for a cluster containing i vacancies can be calculated from

$$E^b(i) = E^f(i-1) + E^f(1) - E^f(i). \tag{13}$$

The results of such calculations, are shown in Figure 7, demonstrate that the binding energy of vacancy clusters is a non-monotonic function of the cluster size and cannot be expressed simply in term of nearest-neighbor interactions [39, 44]. Similar to tight-binding calculations for silicon [41], some of germanium HRC vacancy clusters ($i = 5, 8, 12, 16, 18, ...$) display higher

Table 1: Binding energy (eV) of i isolated vacancies after the reaction $iV \rightarrow V_i$.

$2V \rightarrow V_2$	$3V \rightarrow V_3$	$4V \rightarrow V_4$	Reference
1.48	2.40	3.65	[8]
1.10	1.97	2.70	[45]

stability (i.e. a higher $E^b(i)$) than clusters with an exact number of six-member rings ($i = 6, 10, 14, 18, ...$). Bongiorno et al. [41] proposed a two step explanation for such behavior in silicon. The first step is to select those aggregates obtained by extracting atoms from complete six-member rings. A structure formed in this way minimizes the number of dangling bonds created at the cluster boundary and, in turn, minimizes the internal surface energy along the $< 111 >$ or equivalent direction (it is well known that the (111) surface in the diamond lattice corresponds to the minimal surface energy). The second step addresses the relaxation features of the internal surface. The rearrangement of the dangling bonds favors in some cases a cluster which does not strictly fulfill the previous topological conditions. This is the case for cluster with sizes $i = 5, 8, 12, 16$ in which the structural rearrangement modifies the number of dangling bonds with respect to the unrelaxed structure. In any case, the aggregation of a new vacancy to a stable cluster always gives rise to a less stable structure, as is the case for $i = 7, 11, 15, 19$. A similar relaxation process is observed for SPC clusters, which contain 5, 8, 10, 14, 16, 19 vacancies. In this case the (100) internal surfaces are relaxed as well.

The binding energy of 1.48 eV for the germanium di-vacancy obtained in this work from MD calculations is in good agreement with the value of 1.5 eV obtained by Janke et al. [46] who used DFT in a cluster method. It is higher than the 1.1 eV obtained by Sueoka and Vanhellemont [45] who employed supercell DFT LDA/GGA calculations.

However, Sueoka and Vanhellemont [45] used a different equation for calculating the binding energy. They calculated binding energy of i isolated vacancies through the reaction $iV \rightarrow V_i$ up to $i = 4$, while (13) determines binding energy of isolated single vacancy and $i - 1$ vacancy cluster through the reaction $V + V_{i-1} \rightarrow V_i$. In order to compare MD results obtained here with Sueoka and Vanhelemont estimates, the binding energy of isolated i vacancies was calculated, according to the following equation

$$E^b_{isolated}(i) = iE(N - 1) - [E(N - i) + (i - 1)E(N)], \qquad (14)$$

where, $E(N)$ is the enthalpy of a perfect lattice with N atoms, $E(N - i)$ is the enthalpy of a system with $N - i$ atoms (lattice with N sites and i vacancies).

The results of these calculations are shown in Figure 7 for a cluster size up to 35 vacancies. Table 1 shows that the binding energies calculated for the smaller clusters are higher than the values reported by Sueoka and Vanhellemont [45]. One reason for this difference might be the small supercell of 64 Ge atoms in a perfect lattice that was used in the DFT calculations. The choice of a sufficiently large supercell is important for accurate binding energy estimation, because of the lattice relaxation around a vacancy and vacancy clusters, as has been shown previously for silicon [47, 48]. Even though the relaxation intensity decays rapidly away from the vacancy, it decreases more slowly along the zigzag chain of atoms in the $< 110 >$ directions. The same lattice relaxation as in silicon, which is significant up to the fifth shell of the nearest-neighbor atoms around the vacancy,was observed for germanium [49].
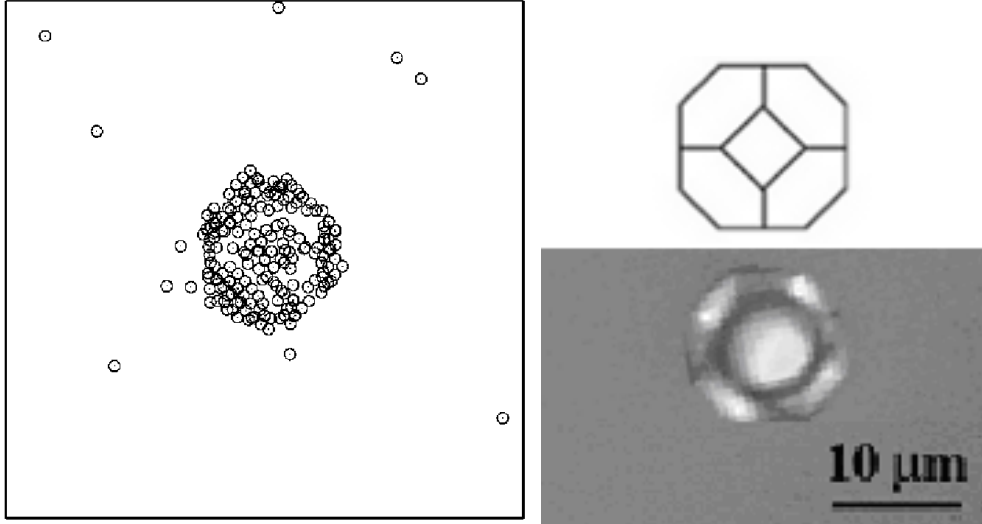
Figure 8: **Left**: Atoms in the vicinity of the 314-vacancies cluster in germanium, as viewed along the $< 001 >$ direction, with the square displacement exceeding 22 pm. The frame indicates the edges of the computational domain [8]. **Right**: Optical micro-graph a a "Crystal Originated Particle" or COP on a polished germanium wafer. The COP originates from a truncated octahedral void in the bulk of the as-grown Cz germanium crystal schematically shown on top.

7.3 MD simulation of the equilibrium shape of a cluster of 314 vacancies

Molecular dynamics simulations were also performed for a large vacancy cluster. A perfect germanium lattice site containing 46656 atoms was used to create a spherical vacancy cluster containing 314 vacancies. A SW potential with the parameters of Wang and Stroud [50] was used in a 2 ns molecular dynamics annealing run at 1100 K, allowing the cluster to relax and take the shape with the lowest total energy. Similar to the previous simulations, the NVT-ensemble with periodic boundary conditions was employed. The result of the simulation of this very large cluster is shown in Figure 8 and suggests that the vacancy cluster morphology converges to a (truncated) octahedral shape, which is bounded by the low energy (111) and (100) planes. This is in agreement with the experimentally observed surface pit shape on polished germanium wafers [1, 51].

8 Void formation in Cz silicon and germanium

8.1 Simulation of void formation

Simulation of void formation in Cz silicon is well established and several simulators are available. Most of these simulators can also be used with success for germanium if the correct material properties are introduced as was illustrated [52] using the software that was developed by Sinno and Brown [53] for silicon. A dedicated defect simulator was in the mean time developed based on the approach that was used for silicon by Kulkarni and Voronkov [54] to quantitatively predict void generation in Cz germanium crystals [8]. The simulator can be used both for steady state and unsteady state crystal growth.
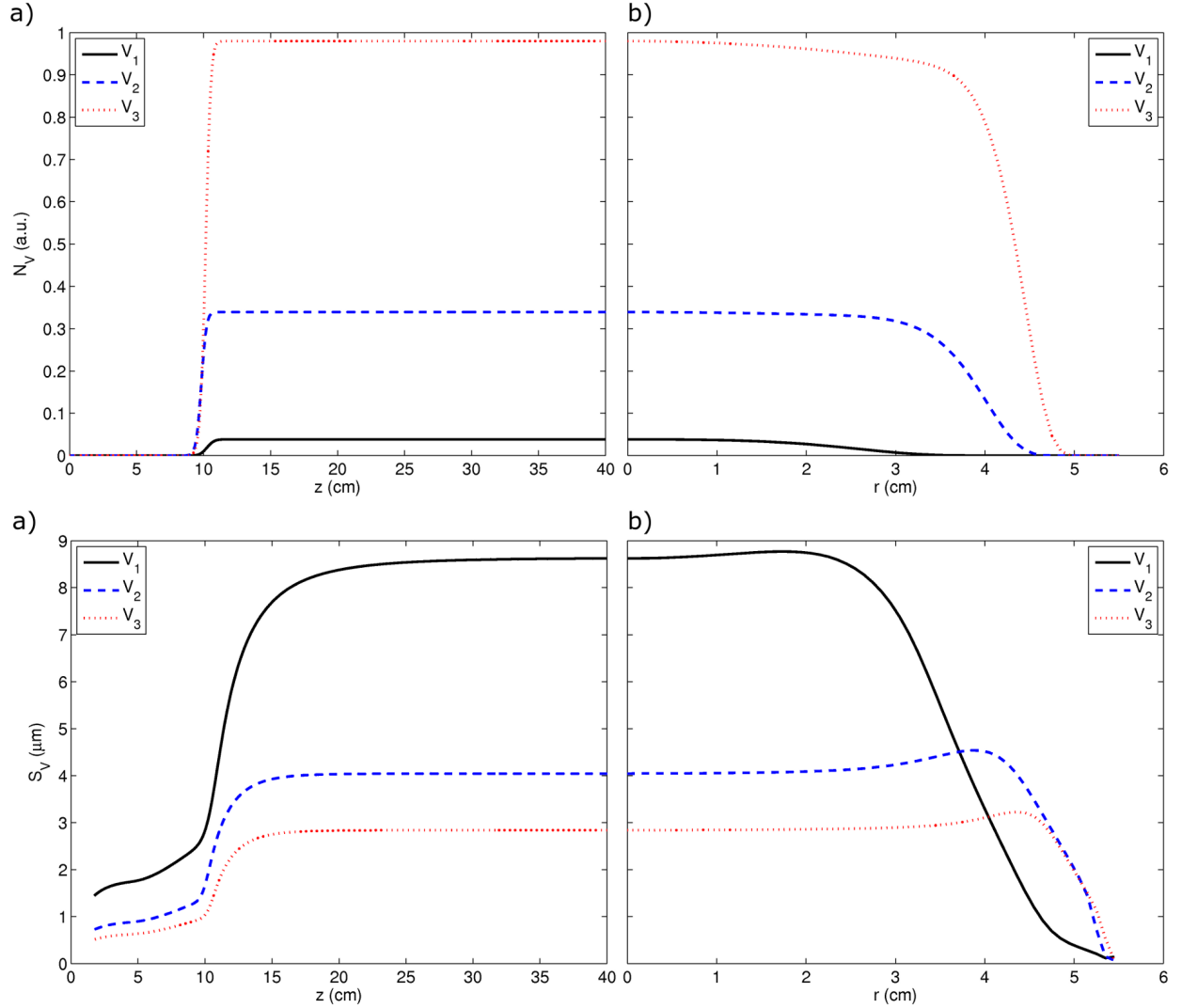
12

Figure 9: **Top**: Comparison of a) axial and b) radial concentrations of voids (N_V) at a crystal length of 40 cm obtained with the aggregation software for pulling speeds $V_1 < V_2 < V_3$. **Bottom**: Comparison of a) axial and b) radial sizes of voids (S_V) at a crystal length of 40 cm (arbitrary units are used for S_V) [8].

8.1.1 Steady state simulations

Examples of steady state simulations are given in Figure 9 showing the axial and radial void size/density distribution at a 4 inch Cz germanium crystal length of 40 cm. A good quantitative agreement is obtained with observed COP size/density distributions on polished germanium wafers [8].

8.1.2 Unsteady state simulations

Unsteady conditions describe that part of growth where pulling conditions are changing with time e.g. the pulling rate changes during the crystal growth, or the diameter of the growing crystal is changing as is the case during crown and end cone forming at the beginning and at the end of the pulling process, respectively. As an example the top of Figure 10 shows the calculated vacancy cluster distribution when the growth rate is continuously decreasing. The

influence of the crystal surfaces on the vacancy cluster distribution is clearly visible, especially at the crown of the crystal. In agreement with steady state simulations reported for silicon, the present calculations also show a decrease of the vacancy cluster density with decreasing growth rate while at the same time the void size increases. This is also illustrated in Figure 11 showing the axial concentration and size of vacancy clusters.

Another illustration of the usefulness of unsteady state calculations is shown in the bottom part of Figure 10. To explain the influence of the crown and end cone of the crystal on the vacancy cluster distribution, unsteady state calculations were performed for a 8 inch crystal grown with constant pull rate. The two-dimensional distributions of temperature (T), vacancy concentration (C_V), vacancy cluster concentration (N_V) and vacancy cluster size (S_V) are shown. The superimposed axial concentration and size of vacancy clusters are shown in Figure 11.

The effect of vacancy cluster dissociation is more pronounced during the end cone formation of the crystal at the end of the pulling process. This can be understood by the reduction of the source of vacancies from the crystal/melt interface because this area is continuously shrinking.

8.2   SIRM study of voids in Cz silicon and Ge doped Cz silicon

Figure 12 summarizes the main results obtained in a recent study with Scanning Infra Red Microscopy (SIRM) of voids in as-grown Cz silicon and Ge doped Cz silicon crystals [55]. Previously published void diameter-density relations in 6 and 8 inch crystals are superimposed on the SIRM measurement results in the right hand figure [56, 57]. The 6 and 8 inch diameter wafers in that previous study were boron-doped (001) wafers labeled A to D whereby the pulling speed decreases from A to D. The resistivity range and oxygen content were comparable to those of the present study while the calculated ratio of the pulling rate over the temperature gradient was well above the critical value of $0.13 \, \text{mm}^2 \, \text{K}^{-1} \, \text{min}^{-1}$ so that vacancy-rich crystals were grown in all cases, leading to the formation of voids during crystal cooling. These published Infra Red Light Scattering Tomography (IR-LST) void sizes were recalculated in the present paper assuming spherical voids instead of octahedral ones like is also assumed for the interpretation of the SIRM data. This yields a void radius that is about 48 % of the edge size of the octahedron. The agreement with the old data for 6 inch crystals is excellent in particular when the average values of the present study are considered. The average results for the two 6 inch crystals used in the present study are also very close to each other leading to the conclusion that there is no significant impact of $10^{18} \, \text{cm}^{-3}$ Ge doping and that void size and density are mainly determined by the pulling conditions. The fact that void size and density in the 4" crystal with a 100 times higher Ge doping is very close to the 6" results, supports the interpretation that there is little or no effect of Ge doping on the single void size.

Surprising at first sight is that the average single void density and size seems not to depend strongly on the crystal diameter [2]. The main reason is that the crystals were pulled with a pulling rate above 1 mm/min. It is known that for such high pulling rates, the thermal gradient at the melt/solid interface in the center of the crystal is lowered and becomes less sensitive for crystal diameter changes and for differences in hot zone [58, 59].

Multiple void formation seems however to be suppressed by Ge doping when comparing the results for the 6GCZ and 6CZ crystals. On the other hand, the multiple void concentration in the 4GCZ crystal is higher than in the 6GCZ wafer. This is probably due to the higher oxygen concentration in the 4 inch crystal which is comparable to that in the 6CZ crystal. The difference in the multiple void (and thus also FPD) density is therefor related not only to the Ge doping but also and perhaps mainly to the interstitial oxygen concentration. Recently
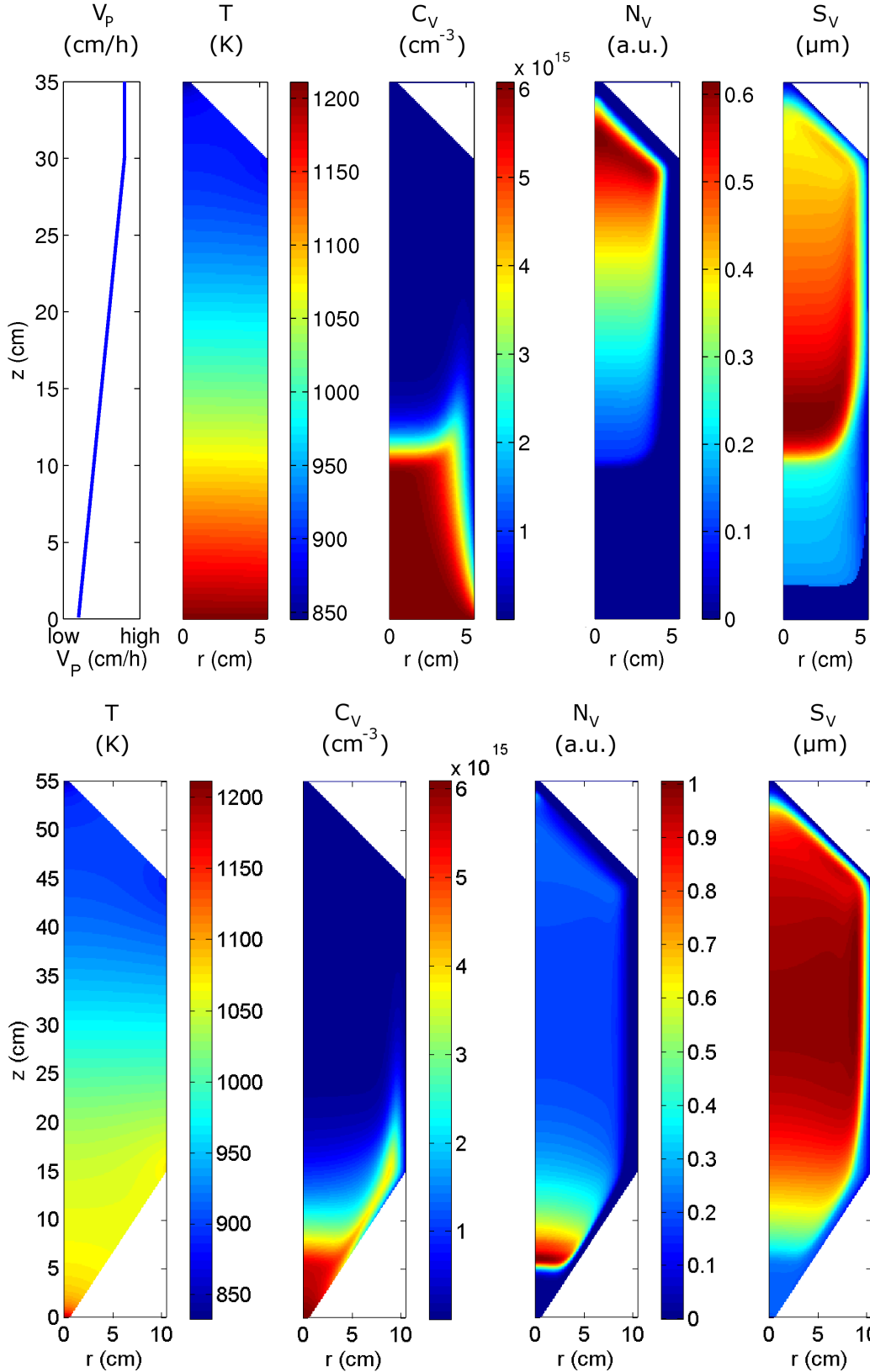
Figure 10: **Top**: Distributions of temperature (T), vacancy concentration (C_V), vacancy cluster concentration (N_V) and vacancy cluster size (S_V) obtained for a continuously decreasing pulling rate (V_P) [8]. **Bottom**: 2D distributions of temperature (T), vacancy concentration (C_V), vacancy cluster concentration (N_V) and vacancy cluster size (S_V) in a 8 inch crystal grown with constant pull rate [8].
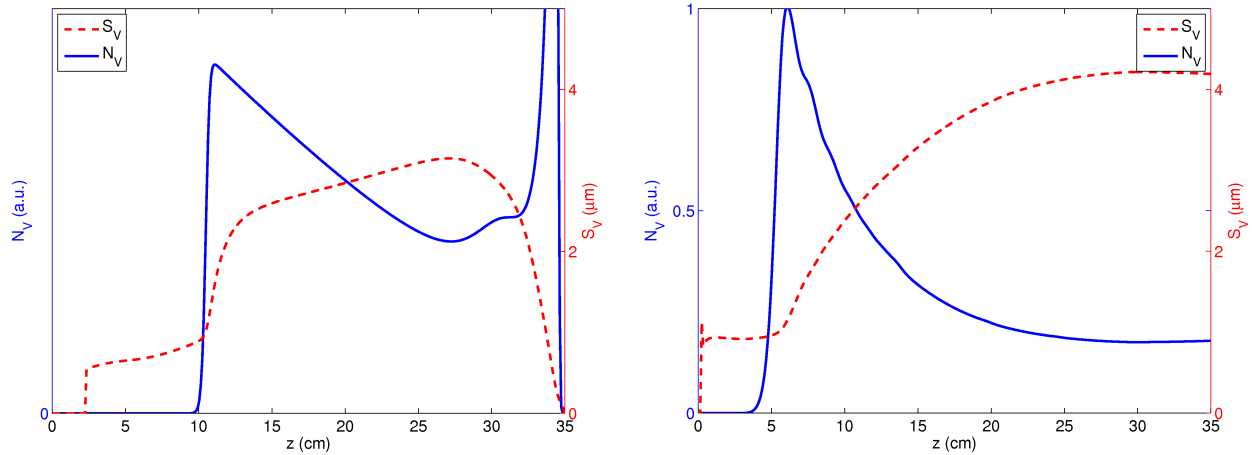
15

Figure 11: **Left**: Axial concentration (N_V) and size (S_V) of vacancy cluster distribution obtained for a continuously decreasing pulling rate [8]. **Right**: Axial concentration (N_V) and size (S_V) of vacancy clusters obtained for a constant crystal pull rate [8].

published results of quantitative modeling of intrinsic point defect and oxygen aggregation during crystal pulling indeed suggest that multiple void formation is enhanced by increasing oxygen concentration [60] as was also suggested previously based on experimental data (see e.g. [56, 57, 60] and references therein). The oxide layer formed on the inner surface of the first void -and thus also the oxygen concentration and that of other impurities in the crystal- plays and important role in the nucleation of the subsequent voids [61, 62].

Although there might thus be an impact of Ge doping on multiple void formation, the results lead to the conclusion that doping with Ge or changing the interstitial oxygen concentration are less effective to control single void formation than doping with nitrogen.

Further more, the reported impact of Ge doping on oxygen precipitation and on thermal donor formation is therefor not due to a reduction of the vacancy concentration immediately after solidification of the crystal, but occurs at the lower temperatures when oxide nuclei are formed. At temperatures below the void nucleation temperature, which is estimated to be in in the range between 1050 and 1100 °C, the free vacancy concentration that is playing a crucial role in oxide precipitate nucleation, might be changed by the presence of Ge atoms due to a.o. a shift of the VO and VO_2 balance by the interaction of Ge atoms with free vacancies and/or interstitial oxygen atoms.

9 Conclusions

There are many similarities between silicon and germanium. A major difference is that during Cz growth of germanium, the vacancy is the dominating intrinsic point defect while for silicon it is relatively easy to grow also self-interstitial-rich crystals.

Due to the dominance of the vacancy in germanium, rapid cooling of heated germanium single crystals creates vacancy-related acceptors caused by the thermal vacancies which are present in equilibrium at the quenching temperature. The obtained thermal acceptor formation energies and deep levels associated with the quenched-in defects are in good agreement with those of different charge states of the vacancy obtained using analytical and ab initio
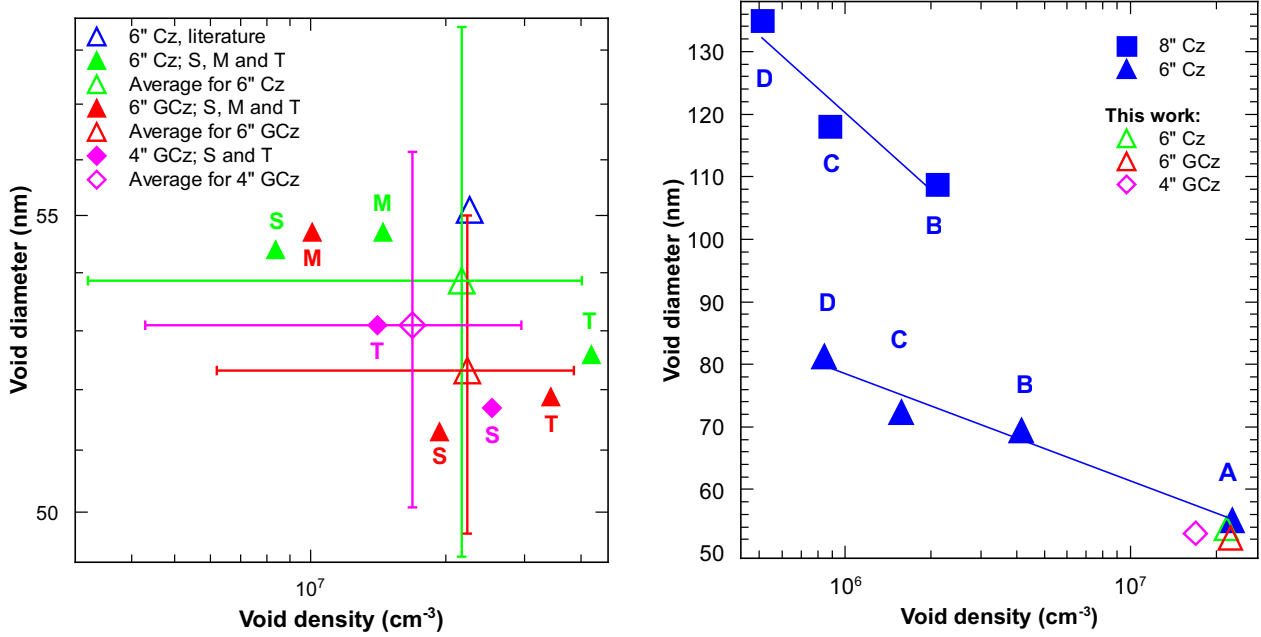
Figure 12: **Left**: SIRM results obtained in the central area of 4 and 6 inch Cz silicon (CZ) and Ge doped Cz silicon (GCZ) wafers. (S = seed-end, M = middle and T = tail-end of the crystal) [2]. A previously published data point for 6 inch Cz silicon crystals is also shown illustrating a very good agreement [56, 57]. **Right**: Published void size-density distributions in 6 and 8 inch crystals [56, 57] whereby the pulling speed decreases from A to D with superimposed the average values obtained in the present study [55].

calculations.

Doping of Czochralski silicon with germanium concentrations up to 1% during the Czochralski pulling process has several advantages as it can enhance oxygen precipitation in low oxygen content material, it suppresses thermal donor formation and it makes the wafers more resistant against breaking during wafering or device processing. The low concentration of germanium has no impact on diode characteristics so that device design does not have to be changed.

Quenching experiments on such Ge doped silicon crystals reveal that the vacancy concentration at high temperatures is little or not affected. This also confirmed by SIRM analyses performed on as-grown silicon and Ge doped silicon wafers revealing only a very limited effect of Ge doping on the void size and density.

Acknowledgements

References

[1] J. Vanhellemont and E. Simoen, J. Electrochem. Soc. **154** (2007) H572.

[2] J. Vanhellemont, J. Chen, W. Xu, D. Yang, J.M. Rafí, H. Ohyama and E. Simoen, submitted for publication in J. Cryst. Growth.

[3] J. Vanhellemont, P. Śpiewak and K. Sueoka, J. Appl. Phys. **101** (2007) 036103.

[4] N. Fukata, M. Suezawa and A. Kasuya, Jpn. J. Appl. Phys. **41** (2002) L1034.

[5] J. Vanhellemont, M. Suezawa and I. Yonenaga, J. Appl. Phys. **108** (2010) 016105.

[6] K. Sueoka, P. Śpiewak and J. Vanhellemont, ECS Transactions **11** (2007) 375.

[7] P. Śpiewak, J. Vanhellemont, K. Sueoka, K.J. Kurzydłowski and I. Romandic, J. Appl. Phys. **103** (2008) 086103.

[8] P. Śpiewak, PhD Thesis, Warsaw University of Technology (2009).

[9] S. Mayburg, Phys. Rev. **95** (1954) 38.

[10] R.A. Logan, Phys. Rev. **101** (1956) 1455.

[11] A.G. Tweet, Phys. Rev. **106** (1957) 221.

[12] A.G. Tweet, J. Appl. Phys. **30** (1959) 2002.

[13] A. Hiraki, J. Phys. Soc. Japan **21** (1966) 34.

[14] A.D. Belyaev, L.I. Datsenko and S.S. Malogolovets, Ukr. Fiz. Zh. **12** (1967) 655.

[15] S. Samuelsson, Ark. Fys. **35** (1967) 321.

[16] L.F. Konorova, Soviet Phys. - Solid State **10** (1969) 2233.

[17] Y. Kamiura, J. Broeckx, P. Clauws, J. Vennik, Solid State Communications **38** (1981) 883.

[18] Y. Kamiura, F. Hashimoto, T. Nobusada, and S. Yoneyama, J. Appl. Phys. **56** (1984) 936.

[19] Y. Kamiura, F. Hashimoto, Jpn. J. Appl. Phys. **28** (1989) 763.

[20] H.H. Woodbury and W.W. Tyler, Phys. Rev. **105** (1957) 84.

[21] E. Simoen, P. Clauws, M. Lamon and J. Vennik, Semicond. Sci. Technol. **1** (1986) 53.

[22] P. Clauws, G. Huylebroeck, E. Simoen, P. Vermaercke, F. Desmet and J. Vennik, Semicond. Sci. technol. **4** (1989) 910.

[23] Y. H. Lee, R. L. Kleinhenz and J. W. Corbet, Appl. Phys. Lett. **31**, 142 (1977).

[24] K. Nakashima, Jpn. J. Appl. Phys. **24**, 1018 (1985).

[25] Y. Kamiura, F. Hashimoto and M. Yoneta, J. Electrochem. Soc. **137**, 3642 (1990).

[26] A. Witecka, Master thesis, Faculty of Materials Science and Engineering, Warsaw University of Technology (2009).

[27] J. Vanhellemont, J. Lauwaert, A. Witecka, P. Śpiewak, I. Romandic and P. Clauws, Physica B: Condensed Matter **404** (2009) 4529.

[28] J. Broeckx, Y. Kamiura, P. Clauws and J. Vennik, Solid State Commun. **40** (1981) 149.

[29] T. Hattori, T. Takada, K. Kawaga, A. Mitsuishi and Y. Kamiura, phys. stat. sol. **120** (1990) K63.

[30] F.A. Kröger, The Chemistry of Imperfect Crystal, North-Holland Publ. Co., Amsterdam, 1964, p.326.

[31] S. Brotzmann and H. Bracht, J. Appl. Phys. **103** (2008) 033508.

[32] P. Śpiewak, K. J. Kurzydłowski, K. Sueoka, I. Romandic and J. Vanhellemont, Solid State Phenomena **131-133** (2008) 241.

[33] H. Bracht, E. E. Haller and R. Clark-Phelps, Physical Review Letters **81** (1998) 393.

[34] Y. Shimizu, M. Uematsu and K. M. Itoh, Physical Review Letters **98** (2007) 095901.

[35] E. Hüger, U. Tietze, D. Lott, H. Bracht, D. Bougeard, E. E. Haller and H. Schmidt, Applied Physics Letters **93** (2008) 162104.

[36] H. D. Fuchs, W. Walukiewicz, E. E. Haller, W. Dondl, R. Schorer, G. Abstreiter, A. I. Rudnev, A. V. Tikhomirov and V. I. Ozhogin, Physical Review B **51** (1995) 16817.

[37] E. Silveira, W. Dondl, G. Abstreiter and E. E. Haller, Physical Review B **56** (1997) 2062.

[38] M. Werner, H. Mehrer and H. D. Hochheimer, Physical Review B **32** (1985) 3930.

[39] M. Prasad and T. Sinno, Applied Physics Letters **80** (2002) 1951.

[40] M. Prasad and T. Sinno, Physical Review B **68** (2003) 045206.

[41] A. Bongiorno, L. Colombo and T. Diaz De la Rubia, Europhysics Letters **43** (1998) 695.

[42] A. van Veen, H. Schut, A. Rivera and A.V. Fedorov, in D.B. Poker, D. Ila, Y.-S. Cheng, L.R. Harriott, and T.W. Sigmon, editors, Ion-Solid Interactions for Materials Modification and Processing, volume 396 of MRS Symposia Proceedings, Materials Research Society, Pittsburgh, 1996, p. 155.

[43] G. H. Gilmer, T. Diaz de la Rubia, D. M. Stock and M. Jaraiz, Nuclear Instruments and Methods in Physics Research Section B: Beam Interactions with Materials and Atoms **102** (1995) 247.

[44] D. J. Chadi and K. J. Chang, Physical Review B **38** (1988) 1523.

[45] K. Sueoka and J. Vanhellemont, Materials Science in Semiconductor Processing **9** (2006) 494.

[46] C. Janke, R. Jones, S. Oberg and P. R. Briddon, Physical Review B **75** (2007) 195208.

[47] C. Z. Wang, C. T. Chan and K. M. Ho, Physical Review Letters **66** (1991) 189.

[48] S. Öğüt, H. Kim and J. R. Chelikowsky, Physical Review B **56** (1997) R11353.

[49] Antônio J. R. da Silva, R. Baierle, R. Mota and A. Fazzio, Physica B: Condensed Matter **302-303** (2001) 364.

[50] Z. Q. Wang and D. Stroud, Physical Review B **38** (1988) 1384.

[51] J. Vanhellemont, P. Śpiewak, K. Sueoka and I. Romandic, in: Proceedings of The Forum on the Science and Technology of Silicon Materials 2007, November 12-14, 2007, Niigata, Japan, eds. H. Yamada-Kaneta ad H. Ono, Shinkousoku Printing Inc., p. 113.

[52] J. Vanhellemont, P. Śpiewak, K. Sueoka, I. Romandic and E. Simoen, in Proceedings of The 5th International Symposium on Advanced Science and Technology of Silicon Materials, Nov. 10-14, 2008, Kona, Hawaii, USA, The Japan Society for the Promotion of Science (JSPS), The 145th Committee, p. 42.

[53] T. Sinno and R. A. Brown, J. Electrochem. Soc. **146** (1999) 2300.

[54] M. S. Kulkarni and V. Voronkov, J. Electrochem. Soc. **152** (2005) G781.

[55] J. Vanhellemont, X. Zhang, W. Xu, J. Chen, X. Ma, and D. Yang, J. Appl. Phys. **108(9)** (2010), in press.

[56] J. Vanhellemont, S. Senkader, G. Kissinger, V. Higgs, M.-A. Trauwaert, D. Gräf, U. Lambert and P. Wagner, J. Cryst. Growth **180** (1997) 353.

[57] J. Vanhellemont, E. Dornberger, D. Gräf, J. Esfandyari, U. Lambert, R. Schmolke, W. von Ammon, and P. Wagner, in: Proceedings of The Kazusa Akademia Park Forum on The Science and Technology of Silicon Materials, (Kazusa Akademia Park, Chiba, Japan, 1997), p. 173.

[58] T. Abe, Mater. Sci. Eng. B **73** (2000) 16.

[59] T. Abe and T. Takahashi, ECS Transactions **335 (11)** (2010) 75.

[60] T. Sinno, J. Dai and S. S. Kapur, Material Science and Engineering B **159-160** (2009) 128.

[61] T. Ueki, M. Itsumi and T. Takeda, Jpn. J. Appl. Phys. **38** (1999) 5695.

[62] T. A. Frewen, S. S. Kapur, W. Haeckl, W. von Ammon and T. Sinno, J. Cryst. Growth **279** (2005) 258.